Article

The Effects of Installation on the Elastic Stiffness Coefficients of Spudcan Foundations

Wen-Long Lin [1,2], Zhen Wang [1], Fei Liu [1] and Jiang-Tao Yi [1,*]

[1] School of Civil Engineering, Chongqing University, No. 83 Shabei Street, Chongqing 400045, China; lwl996ws@163.com (W.-L.L.); zhen.wang@cqu.edu.cn (Z.W.); liufei1991c@163.com (F.L.)

[2] Department of Geotechnical Engineering, Tongji University, Shanghai 200092, China

* Correspondence: yijt@foxmail.com

Abstract: Subjected to pre-load, spudcan foundations, widely utilized to support offshore jack-up rigs, may penetrate in a few diameters into soft clays before mobilizing sufficient resistance from soil. While its stress–strain behavior is known to be affected by the embedment condition and soil backflow, the small-strain calculation with wished-in-place assumption was previously adopted to analyze its elastic stiffness coefficients. This study takes advantage of a recently developed dual-stage Eulerian–Lagrangian (DSEL) technique to re-evaluate the elastic stiffness coefficients of spudcans after realistically modelling the deep, continuous spudcan penetration. A numerical parametric exercise is conducted to investigate the effects of strength non-homogeneity, embedment depths, and the spudcan's size on the elastic stiffness. On these bases, an expression is provided such that the practicing engineers can conveniently factor the installation effects into the estimation of elastic stiffness coefficients of spudcans.

Keywords: spudcan; stiffness; reduction; finite element analysis; dual-stage Eulerian–Lagrangian technique

1. Introduction

Mobile jack-up platforms, extensively used in the offshore industry for drilling and exploration activities, typically consist of three or four retractable lattice legs, each of which is supported by a circular plate-shaped foundation known as a spudcan. To facilitate the assessment of jack-up platforms' ability to withstand storm loading in service, the complex soil–spudcan interaction is usually simplified as the elastic stiffness of the spudcan foundation, which is expressed in dimensionless forms as follows:

$$\left\{ \begin{array}{c} \frac{\delta V}{GR^2} \\ \frac{\delta H}{GR^2} \\ \frac{\delta M}{GR^3} \end{array} \right\} = \left\{ \begin{array}{ccc} K_V & 0 & 0 \\ 0 & K_H & K_C \\ 0 & K_C & K_M \end{array} \right\} \left\{ \begin{array}{c} \frac{\delta w}{R} \\ \frac{\delta u}{R} \\ \delta\theta \end{array} \right\} \tag{1}$$

where R is the radius of spudcan foundation, G is the shear modulus of the soft clay, and K_V, K_H, K_M, and K_C are the mentioned elastic stiffness coefficients. As illustrated in Figure 1, δV, δH, and δM in Equation (1) are in-plane vertical and horizontal force and moment increments, and δw, δu, and $\delta\theta$ are their associated displacement increments, respectively. These elastic stiffness coefficients, i.e., K_H, K_M, and K_C are necessary for structural analysis of the jack-up platform, as they provide boundary conditions. The load–displacement responses of the spudcan, as well as its overlying structure, dynamic response of a jack-up platform, and its natural period, etc., are all affected by these coefficients [1]. Overestimation of them may lead to the underestimation of critical member stresses in places such as the hull–leg connections [2]. Moreover, inaccuracies in the load paths of structures exhibiting significant dynamic effects may arise due to similar overprediction [1,3,4]. Therefore,

a rational estimation/prediction of these elastic stiffness coefficients is of paramount importance to spudcan design practices.
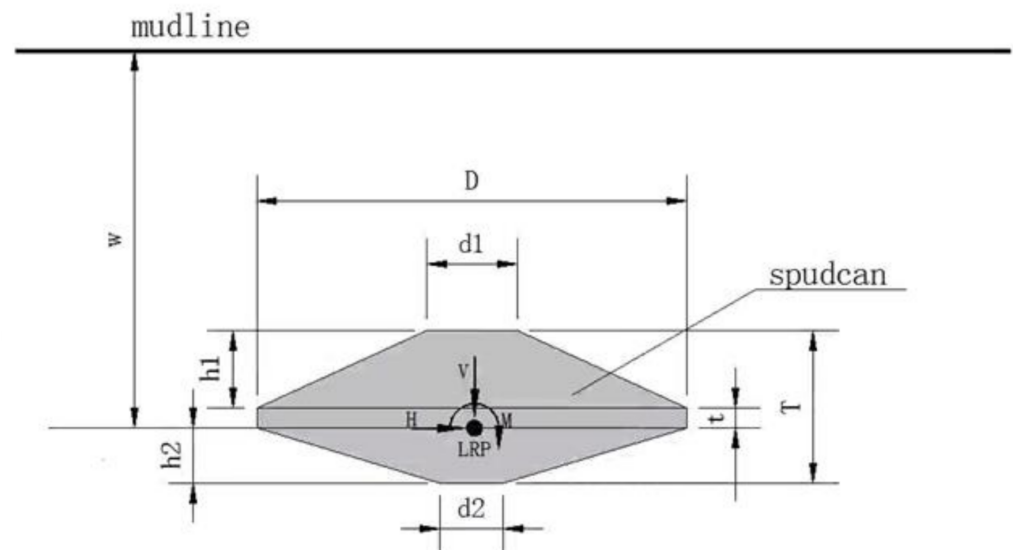
Figure 1. Spudcan foundation and sign conventions for loads and displacements.

In the early years, research attention was directed mainly towards the determination of the elastic stiffness coefficients of rigid circular footings under combined loading conditions on the surface of a homogeneous elastic half-space region [5–7]. Analytical solutions were proposed without the consideration of embedment depth [5]. Later on, after considering the embedment, solutions in matrix form were developed by Bell [6] based on three-dimensional finite element analysis. Ngo-Tran [7] extended Bell's work by providing the elastic stiffness coefficients of rigid conical foundations. Nonetheless, soil was assumed to be homogeneous in the preceding study. Selvadurai [8] calculated the vertical stiffness of a smooth rigid circular foundation in a non-homogeneous half-space region where the shear modulus varied exponentially with depth. Doherty and Deeks [9] used the scaled boundary finite-element method to evaluate dimensionless elastic stiffness coefficients of rigid circular foundations embedded in a non-homogeneous elastic half-space region. Zhang [10] provided the dimensionless elastic stiffness coefficients of a pre-embedded spudcan with buried depths up to several diameters. The non-homogeneity of the soil properties and the back-flow condition of the soil were considered as well. However, the spudcan foundation in Zhang's work was pre-embedded, or wished-in-place, at a certain depth, with the surrounding soil assumed to be in an in situ, or undisturbed, condition. In other words, spudcan installation was not modeled. This clearly contrasts with the reality, where the installation of a spudcan is initiated from the surface, and continues until reaching depths of two to three times its diameter.

Undoubtedly, the foregoing publications contributed substantially to facilitating the understanding of soil–spudcan interaction, modelling the initial stress–strain behavior of spudcan footings, estimating the elastic stiffness coefficients of the spudcan. However, with nearly no exception, the wished-in-place assumption was extensively adopted in this research. Although the analyses could be greatly simplified by ignoring the spudcan deep installation, the soil backflow, cavity formation, and soil disturbance involved, more generally known as "installation effects", were crudely disregarded. These effects are long known to affect various aspects of spudcan behaviors. For example, the bearing capacity of a spudcan under combined vertical (V)–horizontal (H)-moment (M) loading would be significantly decreased if the soil disturbance was considered [11]. By the same reasoning, the installation effects may exhibit themselves on the initial stress–strain behaviors of the spudcan, and, in particular, the elastic stiffness coefficients. In addition, the aforementioned

previous works are by no means complete, and the influence of factors such as spudcan dimensions, soil profile, etc. on the stiffness coefficient have not discussed.

In view of the above, this article intends to re-evaluate the elastic stiffness coefficients of spudcan foundations after the proper consideration of spudcan installation effects. To illustrate the significance of installation effects, both small-strain calculation with wished-in-place assumption and large deformation analyses with consideration of spudcan installation are undertaken. The former is also aimed at augmenting the works of Zhang et al. [10] by the additional consideration of the effects of spudcan size, penetration depth, and soil strength profiles. The latter takes advantage of a recently developed large deformation calculation technique, where the spudcan is penetrated downwards continuously from the surface deeply into soil before VHM loading is applied. Realistic account is thus given to soil backflow conditions. The stiffness coefficients of spudcans, originally derived from small-strain analyses, is then refined after the consideration of installation effects. Reduction factors are introduced to quantify the effect of installation on stiffness.

2. Finite Element Model

2.1. Spudcan Dimenions and Sign Conventions

In the present research, the behavior of spudcan foundations under combined VHM loading is analyzed using generic spudcans with four different dimensions (see Figure 1 and Table 1). In addition, the sign convention adopted throughout the article is illustrated in Figure 1, where, following ISO19905-1 [12], the load reference point (LRP) is taken at the middle of the lowest cross-section of maximum diameter.

Table 1. Dimensions of spudcans adopted in this study.

ID	D (m)	$h1$ (m)	t (m)	$h2$ (m)	$d1$ (m)	$d2$ (m)
Spudcan-I	12	2.43	0.37	1.20	1.57	1.04
Spudcan-II	14	2.92	0.44	1.44	1.88	1.25
Spudcan-III	16	3.41	0.51	1.68	2.19	1.46
Spudcan-IV	18	3.89	0.59	1.92	2.51	1.67

2.2. Soil Strength Profiles

In many offshore sites around the world, soft seabed soil is made of normally consolidated or lightly overconsolidated clay. To model the strength behavior of these soft clayey soils, the strength profile adopted in this study is linear, with undrained shear strength (S_u) increasingly proportionally with depth, as given by the equation below

$$S_u = S_{um} + kz \qquad (2)$$

S_{um}, k, and z are the mudline shear strength, the gradient of soil shear strength, and the depth, respectively. In addition, a uniform stiffness ratio of $E/S_u = 500$ [13] and a constant Poisson's ratio $\nu = 0.49$ are adopted to approximate the undrained condition without incurring numerical instability. As such, the rigidity index $I_r = \frac{G}{S_u}$ is a constant in this study.

2.3. Numerical Simulation Details

As explained earlier, both small-strain and large deformation finite element calculations are conducted in this research. The former has to work in conjunction with the wished-in-place simplification strategy. As depicted in Figure 2, a spudcan is pre-embedded underground with its surrounding soil assumed to be under in situ undisturbed stress conditions. A semi-cylindrical finite element soil model with a diameter and depth of 30D is used here to avoid potential boundary effects [7,14,15] Soil is modeled as Tresca material with undrained shear strength increasing linearly with depth (Equation (2)). The effective unit weight of soil is taken as 6 KN/m^3. The spudcan is modeled as a rigid body with the loads and displacements of the spudcan being related to the LRP. To avoid the

separation between soil and spudcan, and to allow the tensile stress to be developed on the interface, the rigid spudcan is bonded with the soil through the "tie" constraint. This is considered reasonable for the small-strain calculation of the deeply buried spudcan in soft soil, since the suction forces developed on the underside of spudcan can prevent the separation between soil and spudcan during VHM loading. As the small-strain finite element (SSFE) calculations have been widely reported in the literature (e.g., [10,16]), they are not expanded on herein, and the interested readers may find more details from the aforementioned publications. Instead, detailed descriptions will be given regarding the large deformation finite element (LDFE) calculations.
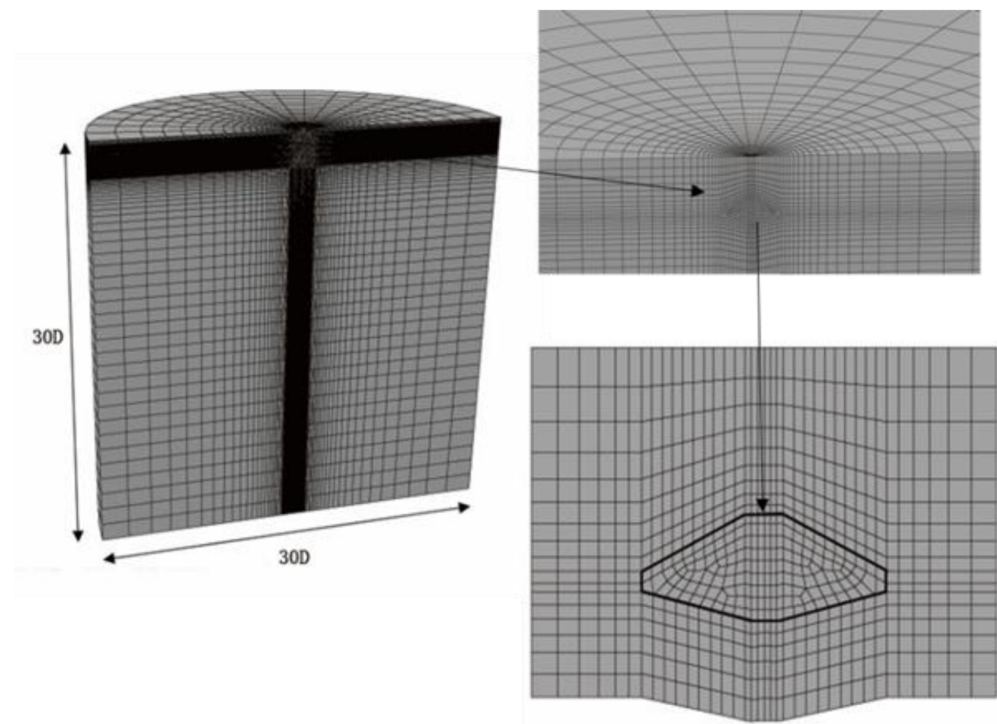
Figure 2. Finite element model for a typical SSFE (small-strain finite element) computation (Spudcan-IV).

In this article, a recently developed LDFE technique, named the "dual-stage Eulerian–Lagrangian (DSEL) technique", is used to continuously simulate the spudcan penetration as well as the subsequent VHM loading. As reported in Yi et al. [17], the entire package of the DSEL program consists of three modules, namely the large deformation Eulerian module, the small-strain Lagrangian module, and the mesh-to-mesh variable mapping module. The large deformation Eulerian module is tailored to solve various undrained, large deformation installation events, while the small-strain Lagrangian module is ideal for analyzing the post-installation behavior characterized by a limited amount of deformation. Therefore, the DSEL technique is well suited to analyzing the problem in question, where the spudcan's continuous penetration is modeled in the first stage by the former and the subsequent combined VHM loading is solved in the second stage by the latter. To bridge between these two stages, the mesh-to-mesh variable mapping module is involved to transfer the calculation results from the end of the first stage to the beginning of the second stage. In this paper, the first stage calculation is executed on the platform of ABAQUS/Explicit, while the second stage analysis is undertaken in ABAQUS/Standard. The solution mapping is conducted outside the ABAQUS environment. Further details about the development of DSEL technique can be found in [17].

Figure 3a shows the finite element model established for the first (Eulerian) stage. In line with the preceding small-strain calculation, soil is modeled as a semi-cylinder with

diameter and depth both equal to 30 times the spudcan diameter. Soil is modeled as a Eulerian domain, where the soil material can move freely without concern of element deformation and distortion; whereas the spudcan is modeled as a rigid body with its load and displacement fully controlled at/determined from the LRP. Again, the constitutive behavior of the soil is modeled via the elastic perfectly plastic Tresca model with linearly increasing strength profiles, which is given as Equation (2). During the continuous penetration of the spudcan at the first stage, complex soil–spudcan interaction is considered through the contacting surfaces, which allow for arbitrary relative separation and frictionless sliding. This is deemed reasonable, since the effect of spudcan roughness on penetration resistance was previously found limited [18,19]. The penetration depth of the spudcan is up to 45 m, and the speed of spudcan penetration is 0.2 m/s. A biased Eulerian meshing algorithm is adopted to improve computational accuracy, where soil around the spudcan is discretized with a finer mesh with a unit size of 0.02D, and coarser meshes are prescribed far away from the spudcan, towards the soil model boundaries.
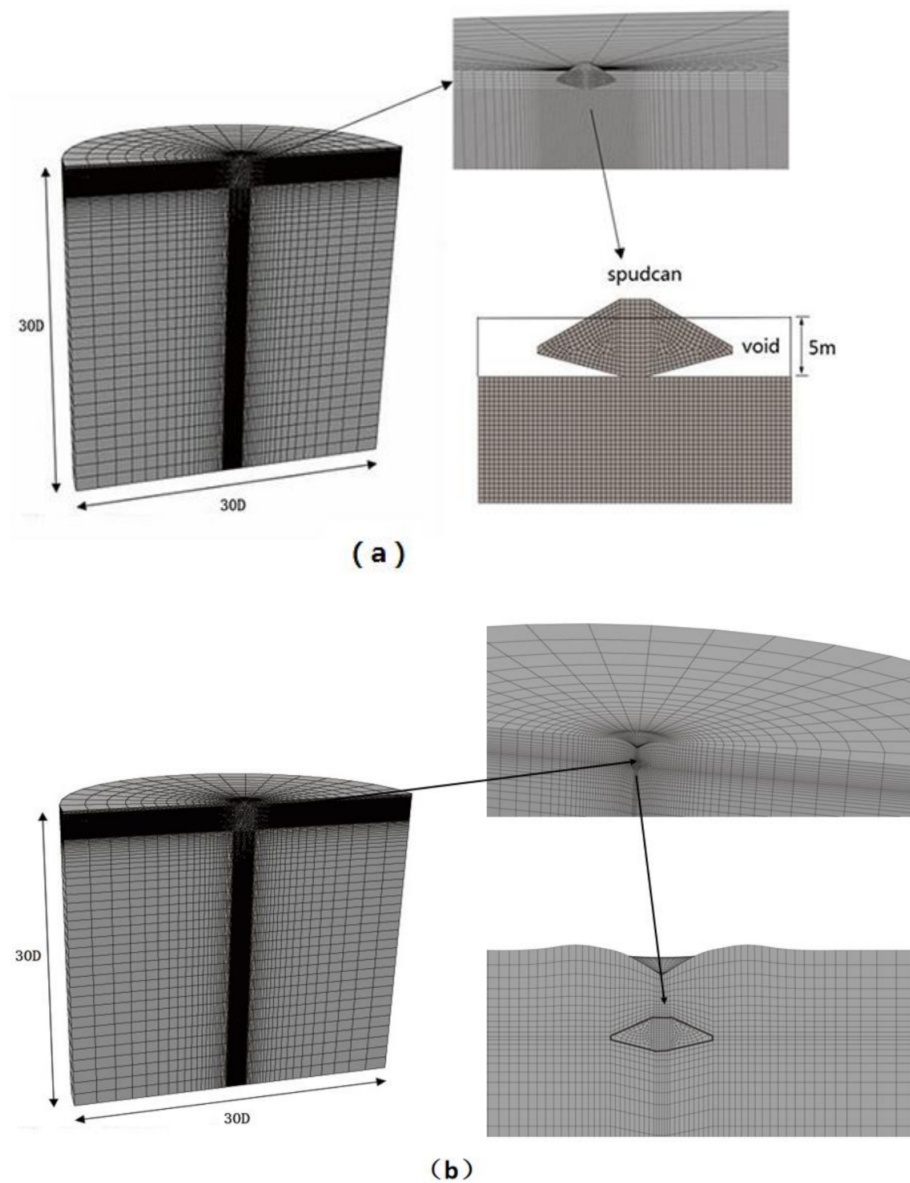
Figure 3. Finite element model for a typical LDFE (large deformation finite element) computation with DSEL (dual-stage Eulerian–Lagrangian) technique (Spudcan-IV): (a) Eulerian finite element model, (b) Lagrangian finite element model.

Upon completion of the first stage of calculation, the deformation geometry of the soil domain is extracted from Eulerian model, which is then used to define the Lagrangian model (Figure 3b) for the second stage. A variety of calculation results, including various stresses components and undrained shear strength, were then transferred from the end of the Eulerian analysis to the beginning of the Lagrangian analysis via the mesh-to-mesh mapping algorithm. For the sake of illustration, Figures 4 and 5 illustrate the Mises stress and undrained shear strength mapped into the Lagrangian model, which are the initial stress and strength condition for the combined VHM loading with the installation effects considered. During the combined VHM loading at the second stage, a bonded soil–spudcan interface is assumed for reasons as previously explained in the SSFE model. The combined VHM loading is then applied in displacement-controlled mode, where displacements along different directions (i.e., w-u-θ) are prescribed at the LRP, and their corresponding loadings (i.e., V-H-M) are read from the calculation results. The elastic stiffness coefficients are thus derived.
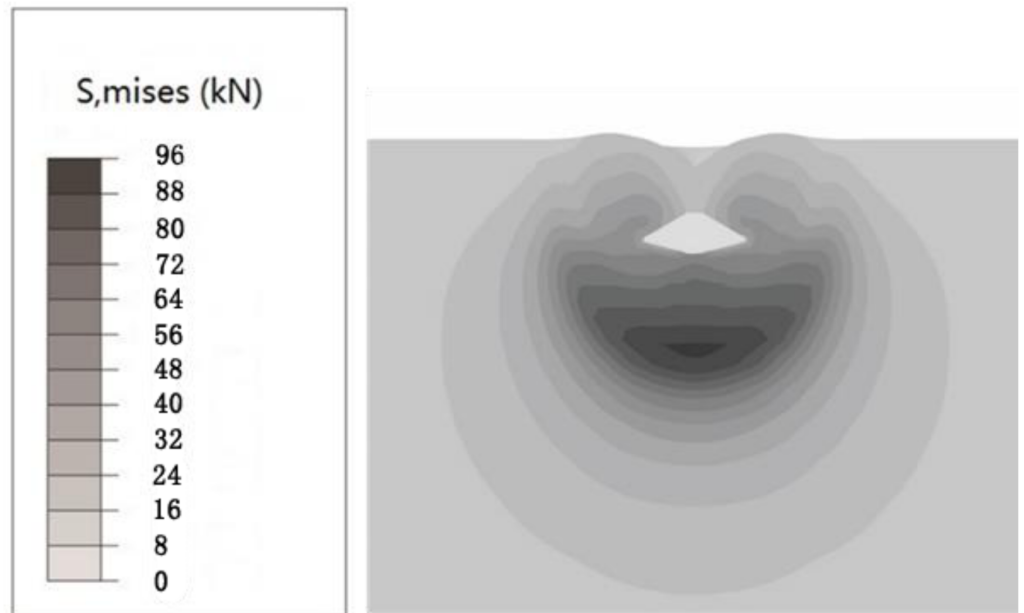
Figure 4. Initial stress field of the small-strain Lagrangian analyses.
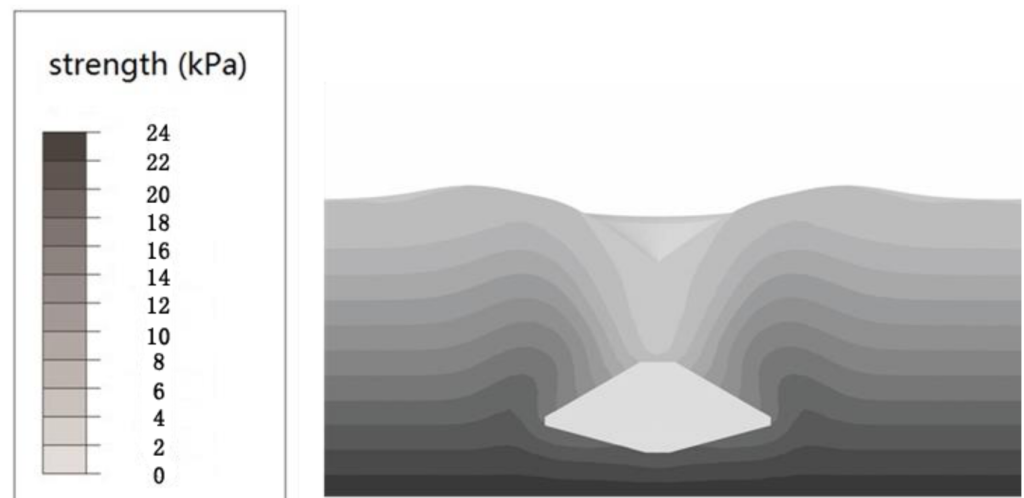
Figure 5. Initial strength field of the small-strain Lagrangian analyses.

One thing should be clarified, although soil is modeled by the Tresca model as an elastic perfectly plastic material, the elastic stiffness coefficients of the spudcan are attained solely from the initial "elastic" responses. In other words, care is taken to ensure the displacement prescribed is sufficiently small to arouse the elastic stress–strain behavior, so as to obtain the initial stiffness of the foundation. In addition, comparison with pure elastic calculation results are made to verify that the initial stiffness computed as such is coincidental with the elastic stiffness, as to be described later on.

2.4. Validation

Due to the lack of analytical solutions for spudcan-shaped footings, the SSFE finite element model is validated by analyzing the surface circular plate footings. The elastic stiffness coefficients calculated by the SSFE finite element model described above is compared with numerical and analytical solutions from the previous publications. The details of these comparisons are provided in Table 2. It is clear that the calculated results are close to the existing solutions, proving the validity of the finite element model.

Table 2. Validation of the finite element model with existing solutions.

		K_V	K_H	K_M
Rough Base	ISO19905-1 [12]	7.843	5.299	5.229
	Zhang [10]	7.955	5.310	5.190
	SSFE of this study	7.924	5.312	5.194
Smooth Base	Zhang [10]	7.954		5.189
	Poulos and Davis [5]	7.843		5.229
	SSFE of this study	7.923		5.192

The validation of the LDFE finite element model is done by analyzing a smooth spudcan penetrating into soil with the shear strength linearly increasing with depth (i.e., Equation (2)). Figure 6 shows the bearing capacity factor (N_c) inferred from the LDFE analysis. A virtually constant value of 12 is reached at a depth greater than 0.5D. This is consistent with the results provided by Hossain and Randolph [18].
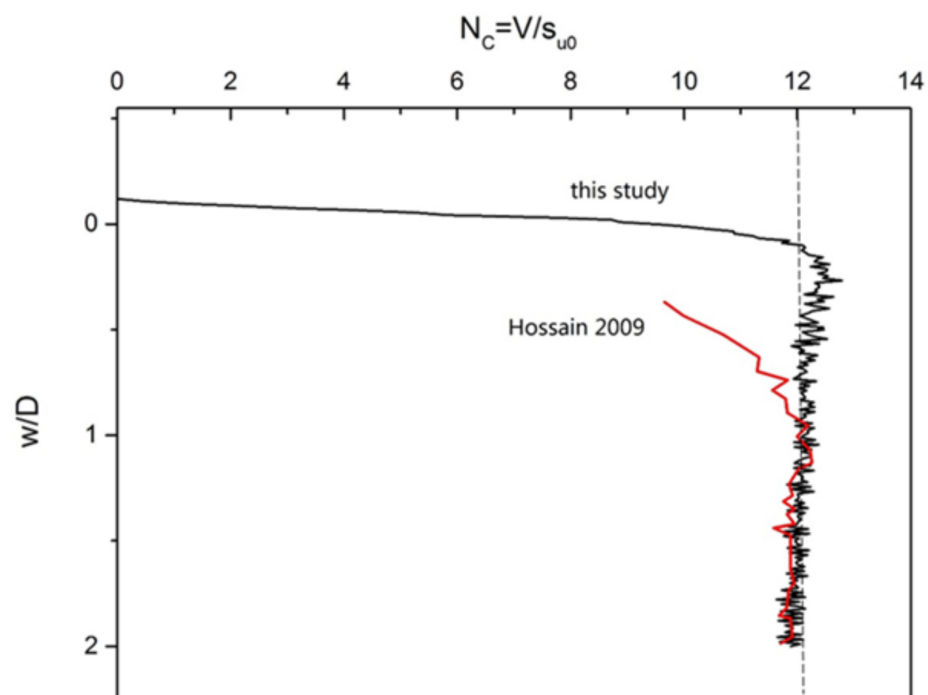
Figure 6. Bearing capacity factor of a smooth spudcan inferred from LDFE calculation with DSEL technique. (S_{u0} in the graph refers to the shear strength at the LRP (load reference point) elevation).

3. Results and Discussion

3.1. Elastic Stiffness Coefficients of Spudcan Without Consideration of Spudcan Installation

To illustrate the installation effects, efforts were first made to explore the elastic stiffness coefficients of the spudcan when the spudcan installation was not considered through the SSFE calculations with a wished-in-place assumption. Basically, they can be largely viewed as an extension to Zhang's work [10], and further considered the effect of strength non-homogeneity, embedment depths, and the spudcan size. A large number (604 in total) of finite element calculations were undertaken, out of which 588 computations provided the database to develop the fitted expressions, and 16 computations served as validation cases to examine the accuracy and reliability of the developed expressions. As shown in Table 3, the 588 computational cases were produced by varying four parameters, namely the strength gradient (k), mudline shear strength (S_{um}), embedded depth of the spudcan (w), and the spudcan diameter (D). As concluded by Zhang et al. [10], their influence can be nicely captured by three normalized parameters, i.e., $\frac{w}{D}$, $\frac{kD}{S_{um}}$, and $\frac{D}{D_s}$. $\frac{w}{D}$ is herein termed the "embedment ratio", $\frac{kD}{S_{um}}$ the "non-homogeneity factor", and $\frac{D}{D_s}$ the "size coefficient". (D_s is the maximum spudcan diameter, which, in this case, is equal to 18 m.)

Table 3. Selection range of the parameter.

Factor	Unit	Selection Range
k (strength gradient)	kPa/m	0.2n, 0.25n, 0.28n, 0.3n (n = 0, 1, 2, 3, 4, 5, 10, 20, 30, 40, 50)
S_{um} (mudline shear strength)	kPa	2.8, 3, 4.8, 5
w (embedded depth of the spudcan)	m	6, 7, 8, 9, 12, 14, 16, 18, 21, 24, 27, 28, 32, 36
D (spudcan diameter)	m	12, 14, 16, 18

Figures 7–9 first show the variation of the initial stiffness coefficients (K_V, K_H, and K_M) with a non-homogeneity factor $\frac{kD}{S_{um}}$ for the several different embedment ratios $\frac{w}{D}$. There are a few observations that are worthy of mentioning. Firstly, when $\frac{w}{D}$ is equal to 0.0, i.e., surface footing, K_V, K_H, and K_M increase dramatically with $\frac{kD}{S_{um}}$ when the latter is less than 5.0. After $\frac{kD}{S_{um}}$ becomes in excess of 5.0, the stiffness coefficients seem to be unaffected by the further increase in $\frac{kD}{S_{um}}$. Secondly, as the footing become increasingly embedded, the variation range of K_V, K_H, and K_M gets continually reduced. In particular, the rotational stiffness coefficient K_M for $\frac{w}{D} = 2.0$ is nearly unchanged as $\frac{kD}{S_{um}}$ varies. That is not illogical, as the stiffness coefficients is affected more by the non-homogeneity within its influenced area. As the embedment depth is deep, the non-homogeneity within its influenced area becomes relatively insignificant.

Figures 10–12 plot the change of K_V, K_H, and K_M with size coefficient $\frac{D}{D_s}$ for several different embedment ratios $\frac{w}{D}$. As can be seen from Figure 10, there is an almost linear correlation between K_V and $\frac{D}{D_s}$, K_V, decreasing nearly proportionally with the increase of $\frac{D}{D_s}$. In addition, the slope of linear trend lines is significantly influenced by the embedment conditions. On the other hand, it is clear from Figures 11 and 12 that K_H and K_M are hardly affected by $\frac{D}{D_s}$. When $\frac{D}{D_s}$ increases from 0.66 to 1, the changes in K_H and K_M are less than 1%.

While only some of the results are illustrated through the preceding graph (Figures 7–12), the entire database obtained from the large number of calculations is fairly large, comprising 588 data. On that basis, fitting excises were carried out with the aid of commercial software "1stopt", which produces the following closed-form expression to account for the combined influences of $\frac{kD}{S_{um}}$, $\frac{D}{D_s}$, and $\frac{w}{D}$:
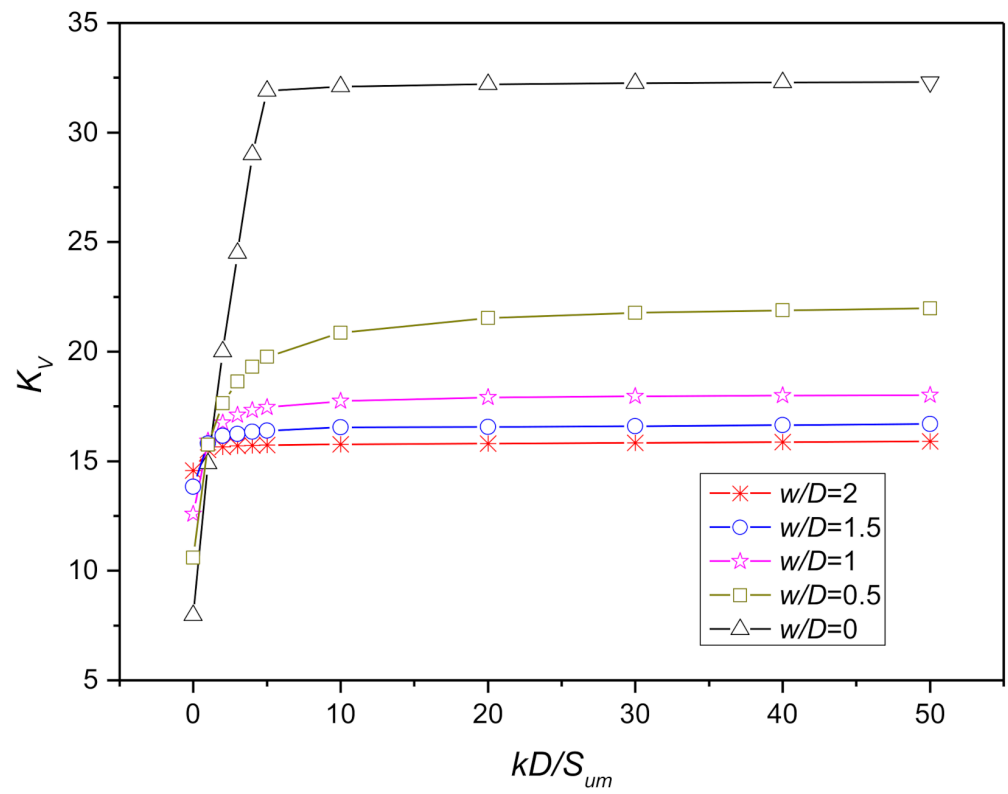
Figure 7. Influence of $\frac{kD}{S_{um}}$ and $\frac{w}{D}$ on K_V when $\frac{w}{D_s} = 1$.
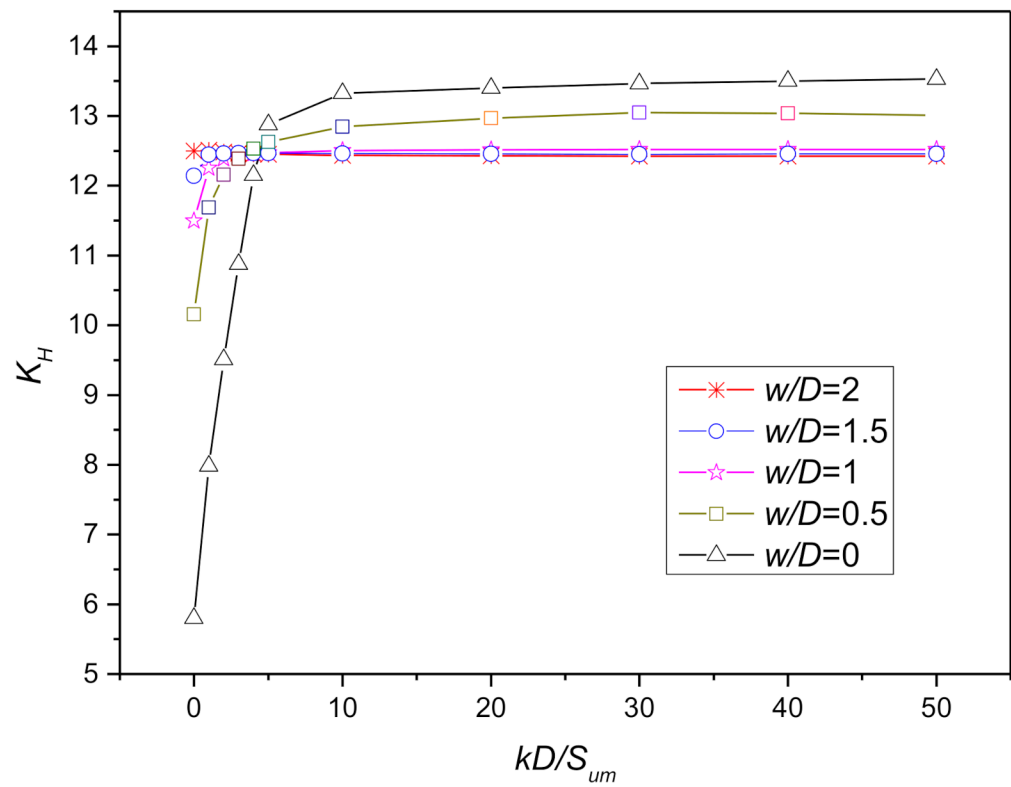
Figure 8. Influence of $\frac{kD}{S_{um}}$ and $\frac{w}{D}$ on K_H when $\frac{w}{D_s} = 1$.
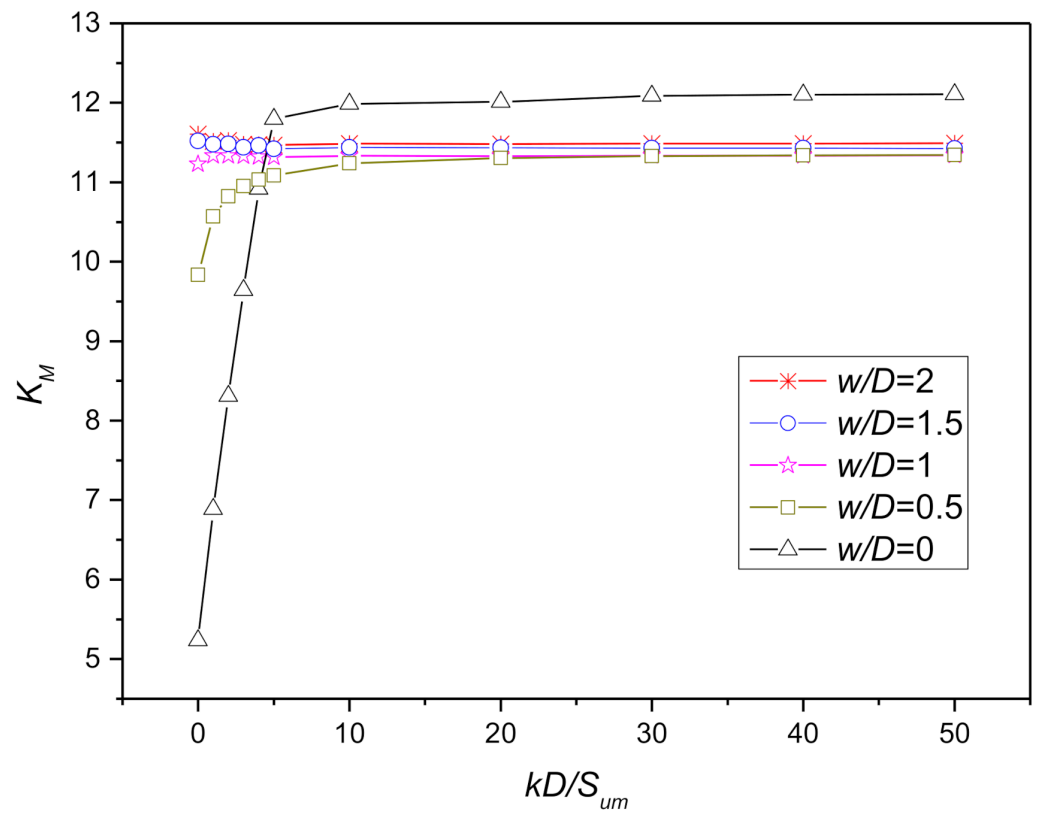
Figure 9. Influence of $\frac{kD}{S_{um}}$ and $\frac{w}{D}$ on K_M when $\frac{w}{D_s} = 1$.
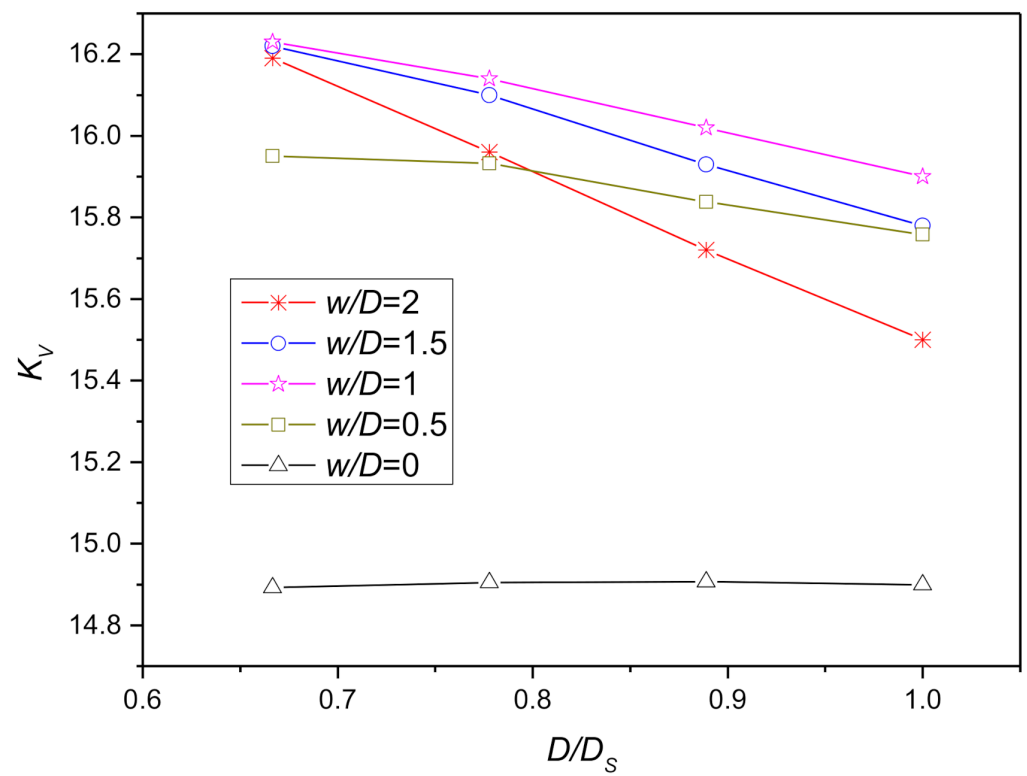
Figure 10. Influence of $\frac{D}{D_s}$ and $\frac{w}{D}$ on K_V when $\frac{kD}{S_{um}} = 1$.
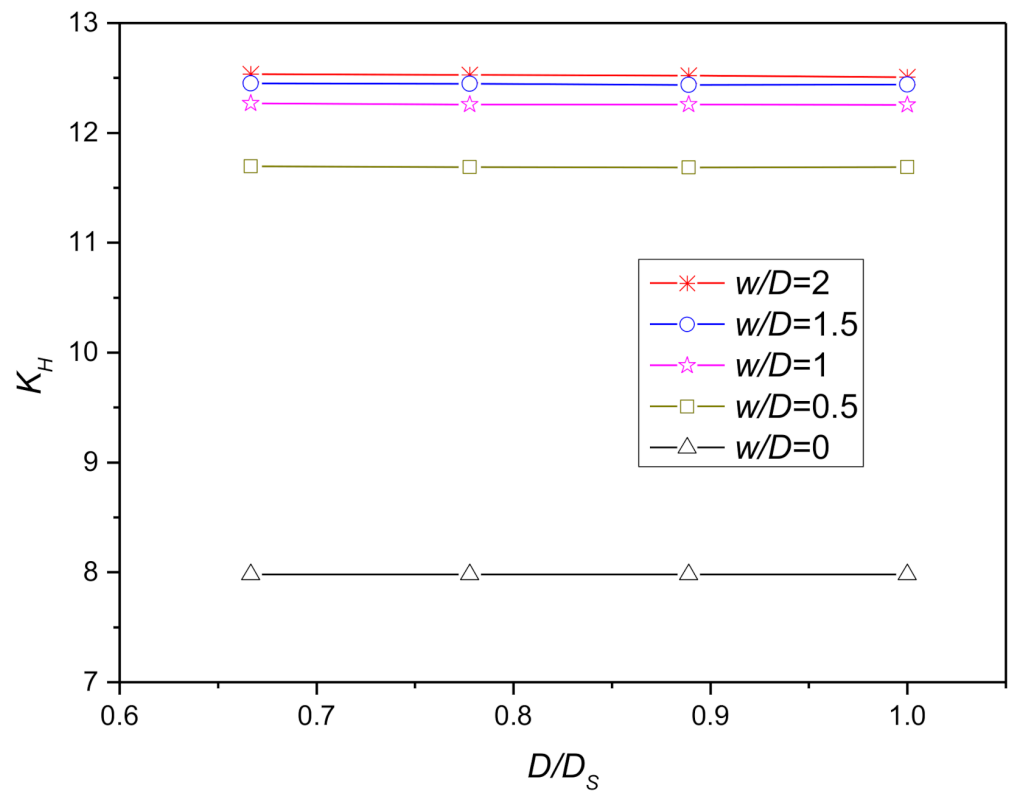
Figure 11. Influence of $\frac{D}{D_s}$ and $\frac{w}{D}$ on K_H when $\frac{kD}{S_{um}} = 1$.
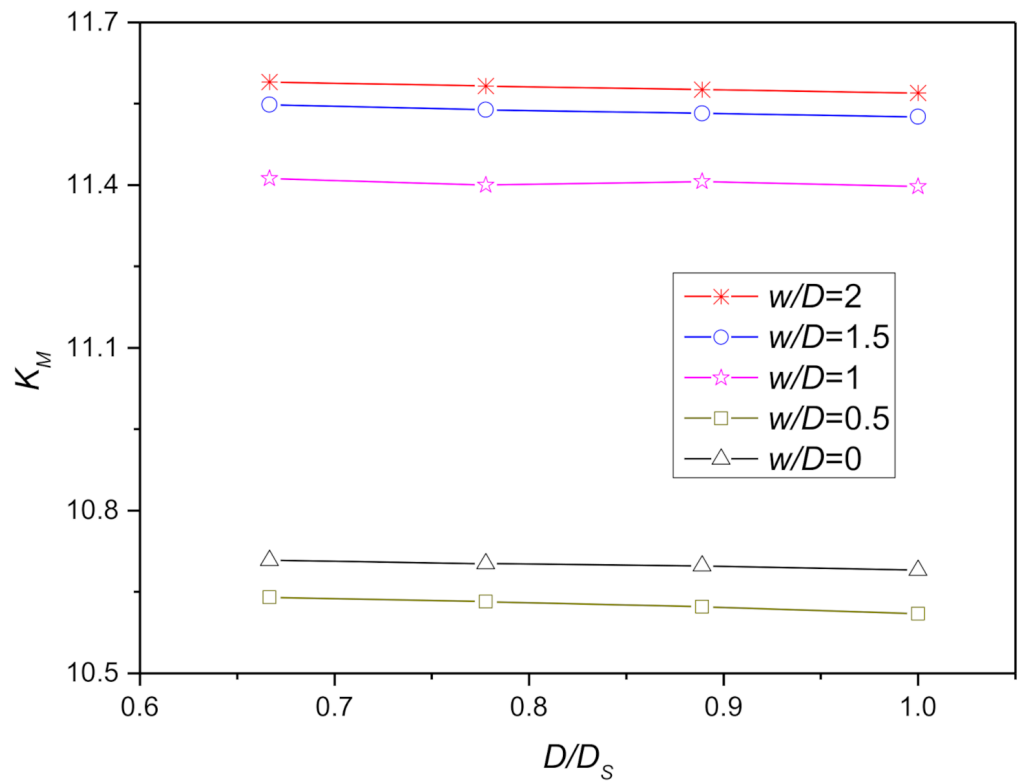
Figure 12. Influence of $\frac{D}{D_s}$ and $\frac{w}{D}$ on K_M when $\frac{kD}{S_{um}} = 1$.

$$K_V = \frac{1 - 0.1\frac{w}{D}\left(\frac{D}{D_S} - 1\right)}{0.069 - 0.037e^{-\frac{w}{D}} + 0.1 * 0.25\frac{w}{D}e^{-0.85\frac{kD}{Sum}}} \tag{3}$$

$$K_H = 13.9 + 0.7^{\frac{kD}{Sum}} * \left(9.4\sqrt{\frac{w}{D}} - 2.5\frac{w}{D} - 8.1\right) - 1.1\sqrt{\frac{w}{D}} \tag{4}$$

$$K_M = 11.4 + \left(0.24 - 6.44\,e^{-2.5\frac{w}{D}}\right)e^{-0.3\frac{kD}{Sum}} \tag{5}$$

Generally, these fitted equations can well reflect the influence of $\frac{kD}{Sum}$, $\frac{D}{D_s}$, and $\frac{w}{D}$ on the elastic coefficients. To illustrate this, the calculation results shown in the preceding Figures 7–9 are compared with the estimations from the Equations (3)–(5), which are then plotted in Figures 13–15. The comparison shows that the expression is in good agreement with the finite element analyses results. To further verify the accuracy of these expressions, the remaining 16 validation computations are taken advantage of. Table 4 provide the full details of these 16 computations. They are constructed based on the orthogonal experimental design, which, in principal, can represent the entire ranges of $\frac{kD}{Sum}$, $\frac{D}{D_s}$, and $\frac{w}{D}$ studied well. The comparison between the calculation's results and estimations from these equations (Equations (3)–(5)) are detailed in Tables 5–7, where the latter are denoted by K'_V, K'_H, and K'_M to differ from the finite element calculation's ones (K_V, K_H, and K_M). On the whole, the difference between the former and latter are subtle, less than 2%. It means that the proposed closed-form expressions can capture the influence of $\frac{kD}{Sum}$, $\frac{D}{D_s}$ and $\frac{w}{D}$ on the elastic stiffness coefficients well.
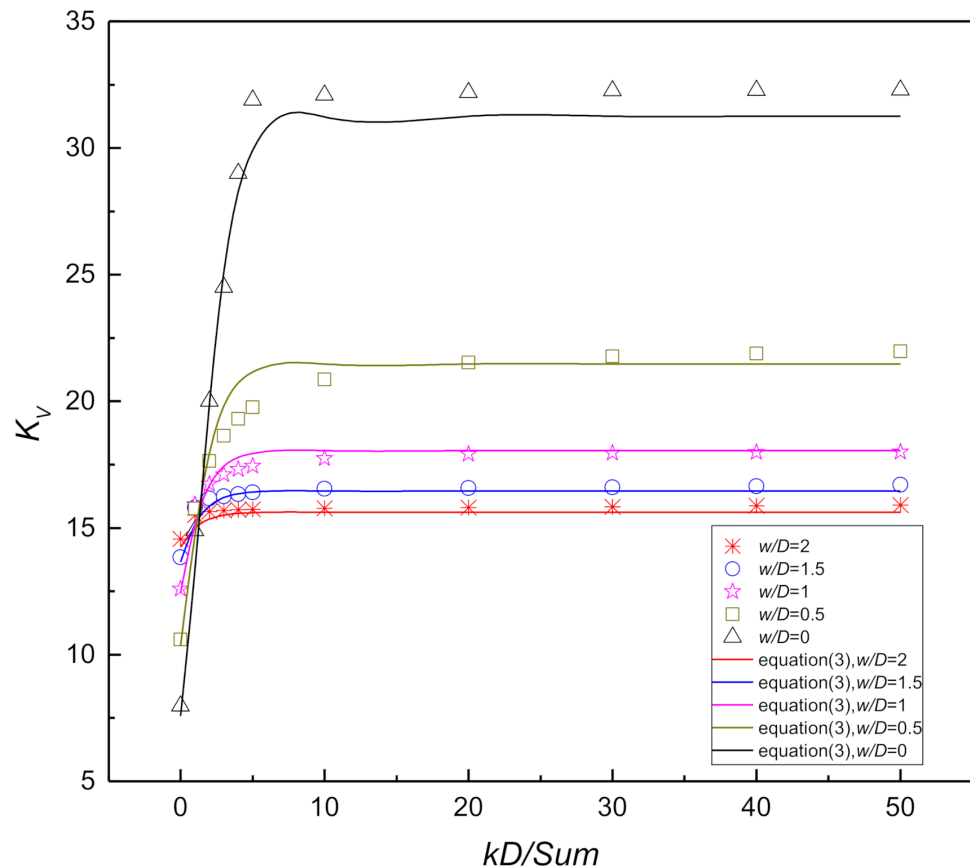
Figure 13. Vertical dimensionless elastic stiffness coefficients with complete backflow of soil.
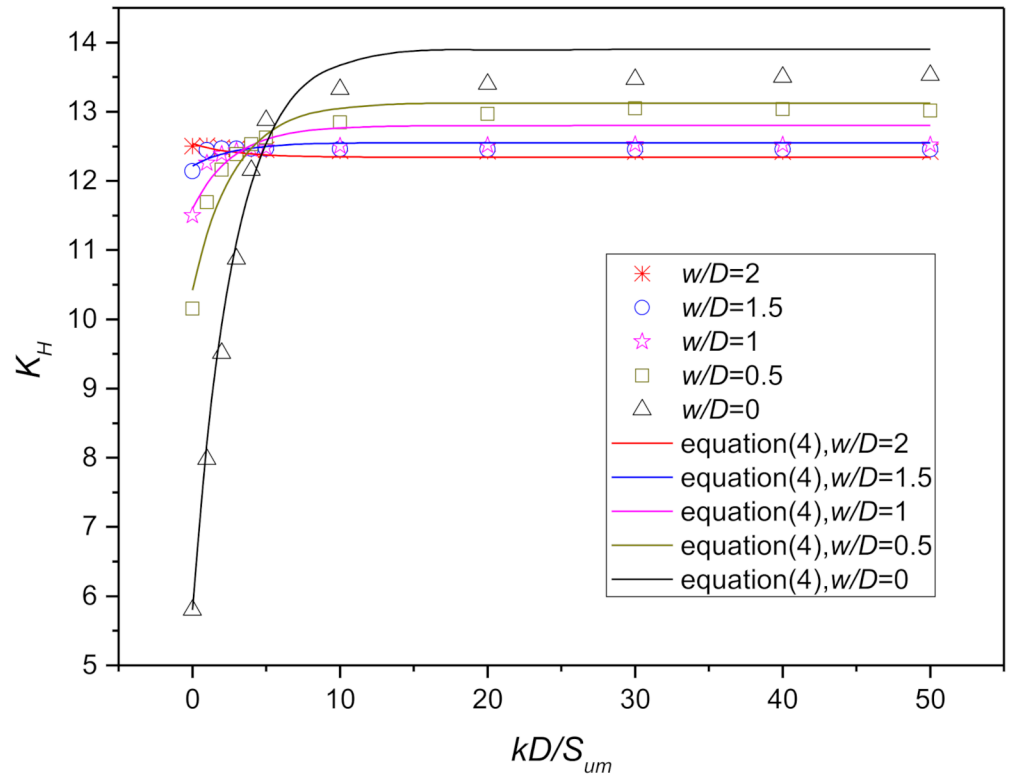
Figure 14. Vertical dimensionless elastic stiffness coefficients with complete backflow of soil.
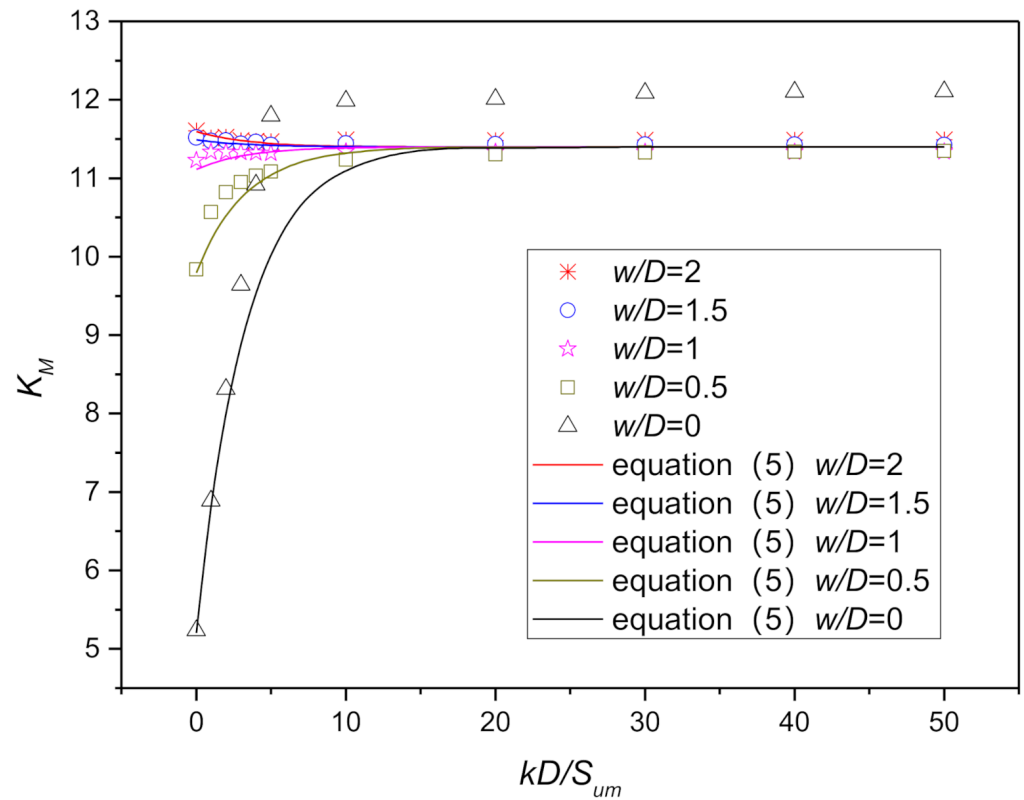
Figure 15. Moment dimensionless elastic stiffness coefficients with complete backflow of soil.

Table 4. Orthogonal experimental design.

Test Number	k (kPa/m)	D (m)	S_{um} (kPa)	w (m)
Test 1	0.28	12	2.5	9
Test 2	0.28	14	5	18
Test 3	0.28	16	7.5	27
Test 4	0.28	18	10	36
Test 5	0.56	12	5	36
Test 6	0.56	14	2.5	27
Test 7	0.56	16	10	18
Test 8	0.56	18	7.5	9
Test 9	0.83	12	7.5	18
Test 10	0.83	14	10	9
Test 11	0.83	16	2.5	36
Test 12	0.83	18	5	27
Test 13	1.11	12	10	27
Test 14	1.11	14	7.5	36
Test 15	1.11	16	5	9
Test 16	1.11	18	2.5	18

As described above, the present analyses were undertaken with the elastic perfectly plastic soil model, where the initial stiffness corresponded to the elastic stiffness. To verify this point, a separate study was conducted where pure elastic material was involved in the calculation. As shown in Tables 8–10, the initial stiffness coefficients of the spudcan embedded in Tresca soil were nearly identical to their counterparts in pure elastic materials ($K_{V,e}$, $K_{H,e}$, and $K_{M,e}$). That is to say, the term "initial stiffness" is interchangeable with "elastic stiffness".

Table 5. Comparison between the vertical stiffness coefficients from expressions and finite element analyses.

Test Number	K_V	$K\prime_V$	Difference (%)
Test 1	16.70	16.32	−2.27
Test 2	15.86	15.26	−3.79
Test 3	15.55	14.99	−3.59
Test 4	15.28	14.69	−3.85
Test 5	15.73	16.26	3.34
Test 6	16.28	16.27	−0.05
Test 7	15.79	15.16	−4.02
Test 8	16.51	16.00	−3.08
Test 9	16.34	16.21	−0.84
Test 10	16.20	15.65	−3.40
Test 11	15.76	15.73	−0.19
Test 12	16.24	16.20	−0.27
Test 13	16.03	16.16	0.82
Test 14	15.70	15.86	1.01
Test 15	19.21	20.06	4.43
Test 16	17.74	18.05	1.72

3.2. Elastic Stiffness Coefficients of Spudcan with Consideration of Spudcan Installation

As explained above, the spudcan, in reality, is continuously penetrated from the surface deeply to a depth of few diameters. The ignorance of installation would preclude the possibility of studying the influence of soil backflow, cavity formation, soil disturbance, etc. These installation effects have been long recognized and widely acknowledged in various aspects of spudcan behaviors. To take account of the installation effect on the elastic stiffness of a spudcan, reduction factors are therefore introduced into the conventional stiffness matrix (Equation (1)), which is re-expressed in the following form:

$$\left\{ \begin{array}{c} \frac{\delta V}{GR^2} \\ \frac{\delta H}{GR^2} \\ \frac{\delta M}{GR^3} \end{array} \right\} = \left\{ \begin{array}{ccc} f_V K_V & 0 & 0 \\ 0 & f_H K_H & K_C \\ 0 & K_C & f_M K_M \end{array} \right\} \left\{ \begin{array}{c} \frac{\delta w}{R} \\ \frac{\delta u}{R} \\ \delta \theta \end{array} \right\} \tag{6}$$

f_V, f_H, and f_M are the reduction factors of K_V, K_H, and K_M, respectively, which are thus indicators of the significance of installation effects. K_V, K_H, and K_M has been earlier demonstrated to be conveniently expressed by Equations (3)–(5). LDFE calculations with the DSEL technique described in Section 2.3 are carried out, the results of which are subsequently processed to figure out the reduction factors f_V, f_H, and f_M.

Table 6. Comparison between the horizontal stiffness coefficients from expressions and finite element analyses.

Test Number	K_H	K'_H	Difference (%)
Test 1	12.20	12.04	−1.32
Test 2	12.34	12.30	−0.32
Test 3	12.45	12.50	0.43
Test 4	12.51	12.66	1.17
Test 5	12.58	12.91	2.59
Test 6	12.51	12.52	0.09
Test 7	12.28	12.25	−0.29
Test 8	11.89	11.85	−0.27
Test 9	12.46	12.41	−0.47
Test 10	12.00	11.91	−0.74
Test 11	12.48	12.54	0.52
Test 12	12.46	12.41	−0.44
Test 13	12.55	12.68	1.07
Test 14	12.53	12.72	1.59
Test 15	12.48	12.37	−0.93
Test 16	12.52	12.41	−0.89

Table 7. Comparison between the moment stiffness coefficients from expressions and finite element analyses.

Test Number	K_M	K'_M	Difference (%)
Test 1	11.22	11.00	−1.96
Test 2	11.49	11.37	−1.07
Test 3	11.56	11.42	−1.17
Test 4	11.57	11.43	−1.18
Test 5	11.60	11.44	−1.42
Test 6	11.52	11.47	−0.42
Test 7	11.44	11.31	−1.11
Test 8	10.72	10.52	−1.86
Test 9	11.52	11.43	−0.80
Test 10	11.02	10.80	−2.03
Test 11	11.53	11.47	−0.52
Test 12	11.44	11.46	0.22
Test 13	11.58	11.45	−1.15
Test 14	11.57	11.45	−1.03
Test 15	11.13	10.89	−2.20
Test 16	11.38	11.40	0.20

Table 8. Comparison between the vertical stiffness coefficients of a spudcan embedded in pure elastic and elastic perfectly plastic soil.

KD/Sum	W/D	$K_{V,e}$	K_V	Difference (%)
0	1	12.492	12.587	0.757
1	1	15.837	15.925	0.554
2	1	16.682	16.739	0.342
3	1	17.188	17.099	−0.520
4	1	17.275	17.313	0.217
5	1	17.465	17.450	−0.086
4	0.5	19.272	19.306	0.176
4	1.5	16.190	16.340	0.928
4	2	15.887	15.724	−1.027

Table 9. Comparison between the horizontal stiffness coefficients of a spudcan embedded in pure elastic and elastic perfectly plastic soil.

KD/Sum	W/D	$K_{H,e}$	K_H	Difference (%)
0	1	11.457	11.497	0.349
1	1	12.335	12.255	−0.649
2	1	12.347	12.385	0.308
3	1	12.429	12.433	0.032
4	1	12.451	12.459	0.066
5	1	12.466	12.474	0.064
4	0.5	12.557	12.532	−0.199
4	1.5	12.459	12.465	0.048
4	2	12.453	12.457	0.032

Table 10. Comparison between the moment initial stiffness coefficients of a spudcan embedded in pure elastic and elastic perfectly plastic soil.

KD/Sum	W/D	$K_{M,e}$	K_M	Difference (%)
0	1	11.221	11.226	0.045
1	1	11.339	11.333	−0.053
2	1	11.345	11.333	−0.106
3	1	11.342	11.327	−0.132
4	1	11.351	11.321	−0.263
5	1	11.323	11.317	−0.053
4	0.5	11.029	11.031	0.018
4	1.5	11.482	11.460	−0.192
4	2	11.530	11.471	−0.511

Figures 16–18 show the reduction factors related to the strength non-homogeneity factor and embedment ratio. Generally speaking, the reduction factors are always less than 1, which implies that the ignorance of installation effects would produce conservative estimations of the elastic stiffness coefficients. The observed decrease or reduction in elastic stiffness after the consideration of installation effects can be explained mainly by several reasons:

Firstly, the penetration of a spudcan commencing from the surface would lead to the gradual formation and development of a cavity, see Figure 19. The absence of soil inside the cavity can then lead to decreases in the stiffness along various loading directions.

Secondly, the installation of the spudcan would, to a large extent, affect and disturb the adjoining soil. The disturbed soil, in turn, contributes to weakening the stress–strain responses, and thus the elastic stiffness of the spudcan, in particular when compared with the in situ conditions.
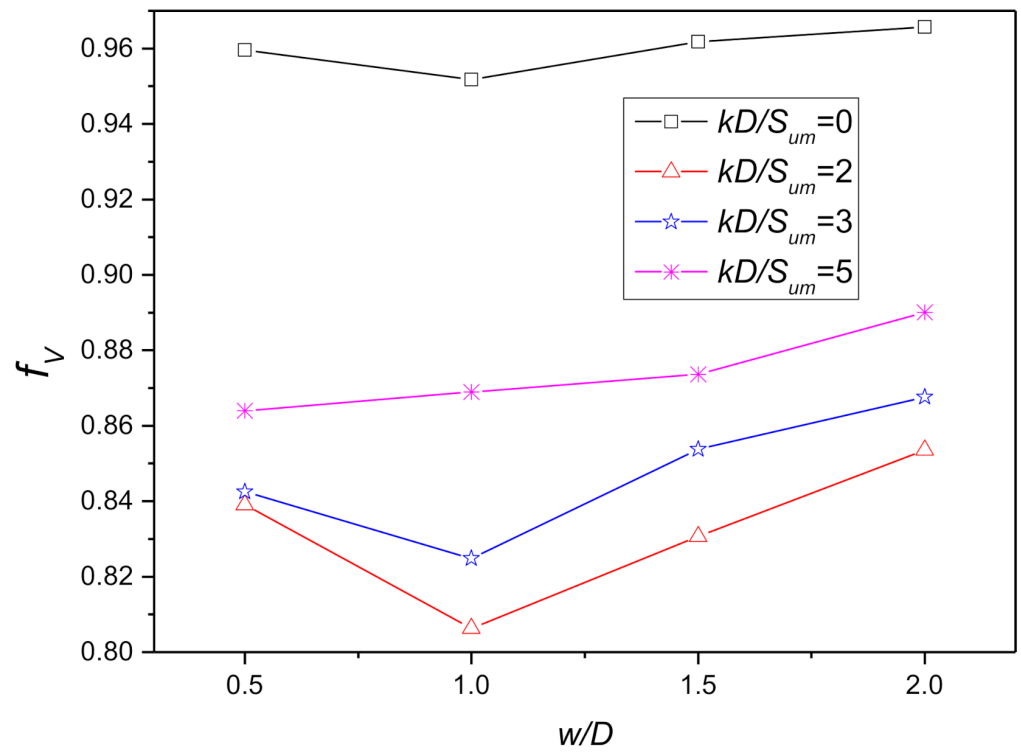
Figure 16. Influence of $\frac{kD}{S_{um}}$ and $\frac{w}{D}$ on f_V when $\frac{D}{D_s} = 1$.
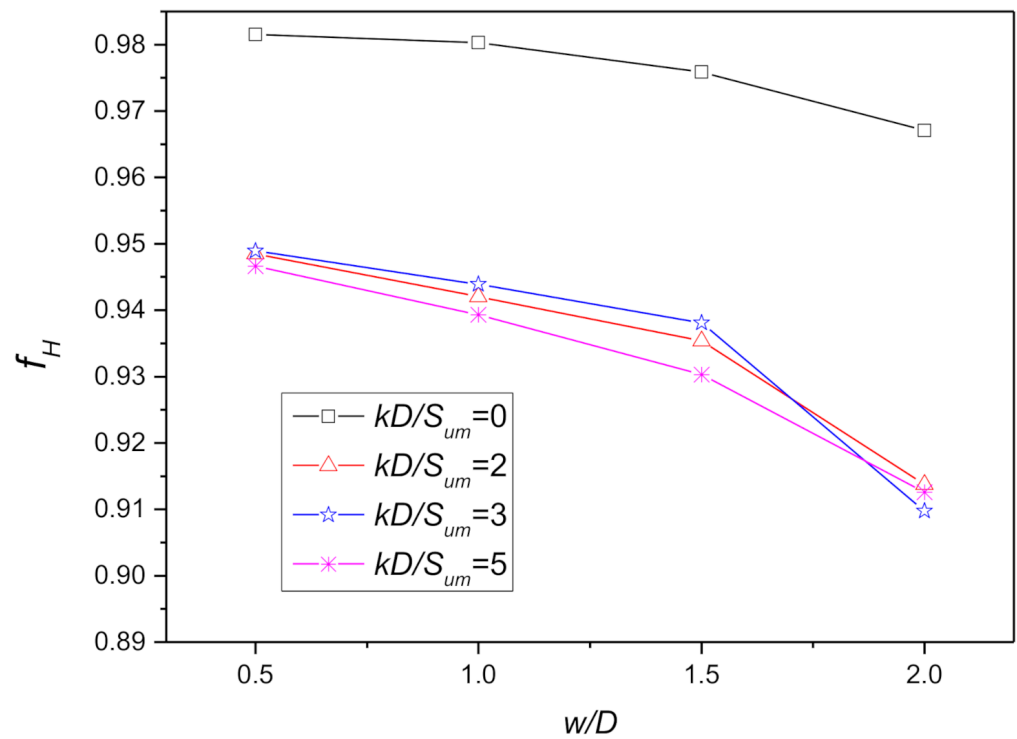
Figure 17. Influence of $\frac{kD}{S_{um}}$ and $\frac{w}{D}$ on f_H when $\frac{D}{D_s} = 1$.
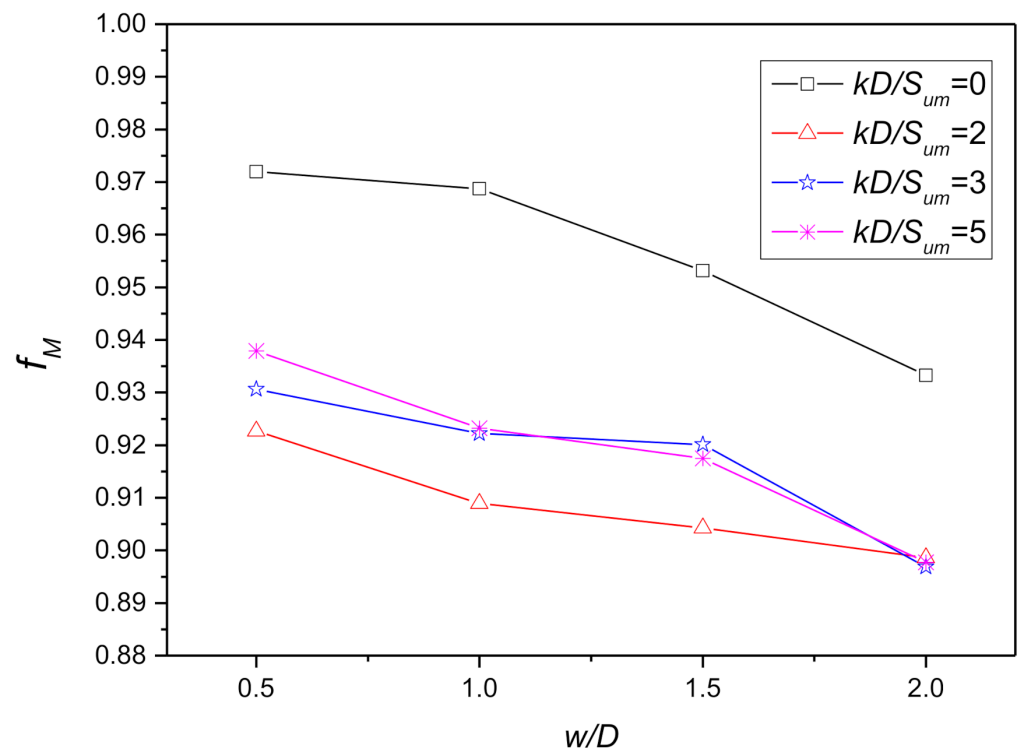
Figure 18. Influence of $\frac{kD}{S_{um}}$ and $\frac{w}{D}$ on f_M when $\frac{D}{D_s} = 1$.

Thirdly, soft soils originally situated on the seabed and at shallow depths would be dragged downward by the continuous spudcan penetration and trapped below the spudcan's underside when subjected to VHM loading. The mechanical properties of these soils are weaker than the original in situ soils. However, the stiffness is calculated by the shear modulus of the in situ soil at the depth of the LRP point, and this shear modulus is larger than the shear modulus of trapped soft soils. As a result, the stiffness coefficient is bound to be reduced.

As far as the vertical elastic stiffness coefficient is concerned (Figure 16), the reduction factor f_V exhibits dissimilar features at different embedment depths. When $0.5 < \frac{w}{D} < 1$, f_V decreases with the increase in $\frac{w}{D}$; whereas f_V clearly increases with $\frac{w}{D}$ when $\frac{w}{D} > 1$. This can be attributed to the occurrence of soil backflow. The penetration of the spudcan is known to be accompanied by significant soil backflow after the critical depth. When the penetration is shallow, say less than 0.5D, the soil backflow does not take place, and the cavity atop the spudcan continually expands in the vertical direction. As a corollary, f_V continually decreases with the increase in the embedment or penetration depth. When the spudcan moves past the critical depth, soil backflow occurs; the backfilled soil moves to cover the spudcan top to provide a seal and limit the further development of the cavity. f_V then senses the change in the cavity volume and increases with the embedment depth.

The reduction factors of horizontal and moment elastic stiffness coefficients, on the other hand, monotonically decrease with the increase in $\frac{w}{D}$, as shown in Figures 17 and 18. This means f_H and f_M are not much affected by the volume of the cavity; instead, they are likely more subjected to the influence of the disturbed soil stress state and trapped weak soils. As the penetration goes deeper, the influence of such disturbed and trapped soils become accentuated. As a result, f_H and f_M consistently decrease with the increase in embedment depth.

Figures 20–22 plot the change of f_V, f_H, and f_M with size coefficient $\frac{D}{D_s}$ for three different non-homogeneity $\frac{kD}{S_{um}}$. As can be seen from these graphs, f_V, f_H, and f_M are affected little by $\frac{D}{D_s}$. When $\frac{D}{D_s}$ increases from 0.66 to 1, the changes in f_V, f_H, and f_M are well within 1%. That is to say, the spudcan size is irrelevant to the reduction factors.
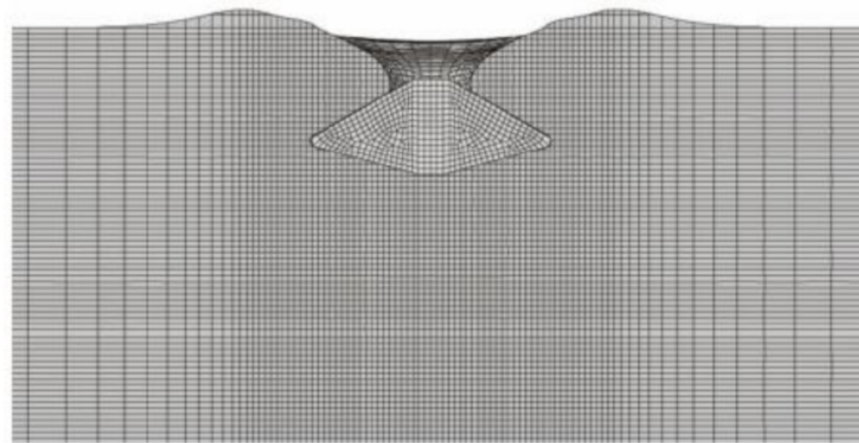
(a) $\frac{w}{D}$=0.5
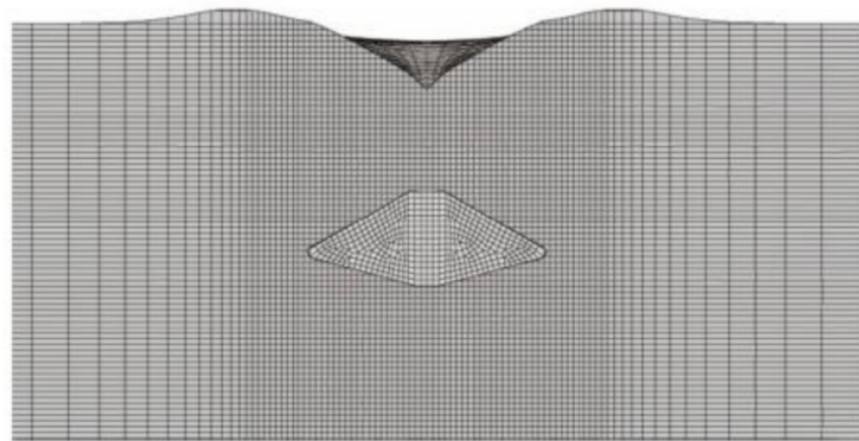
(b) $\frac{w}{D}$=1
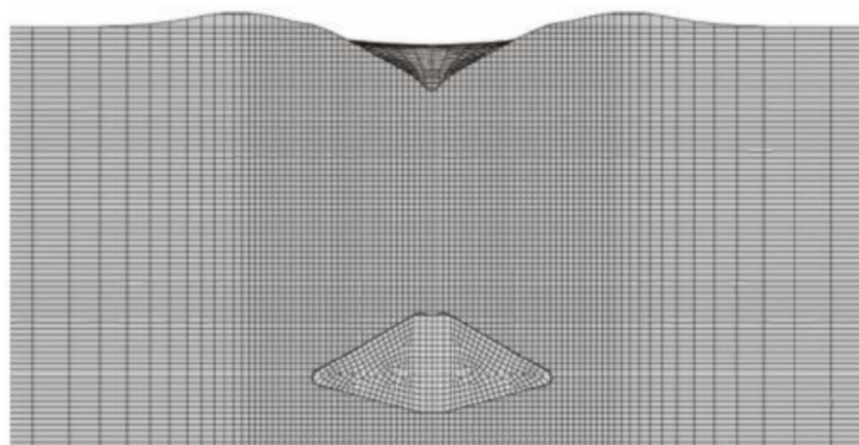
(c) $\frac{w}{D}$=1.5

Figure 19. Cavity at different penetration depths of the spudcan. (Spudcan-IV, $\frac{kD}{S_{um}} = 3$, $\frac{D}{D_s} = 1$.
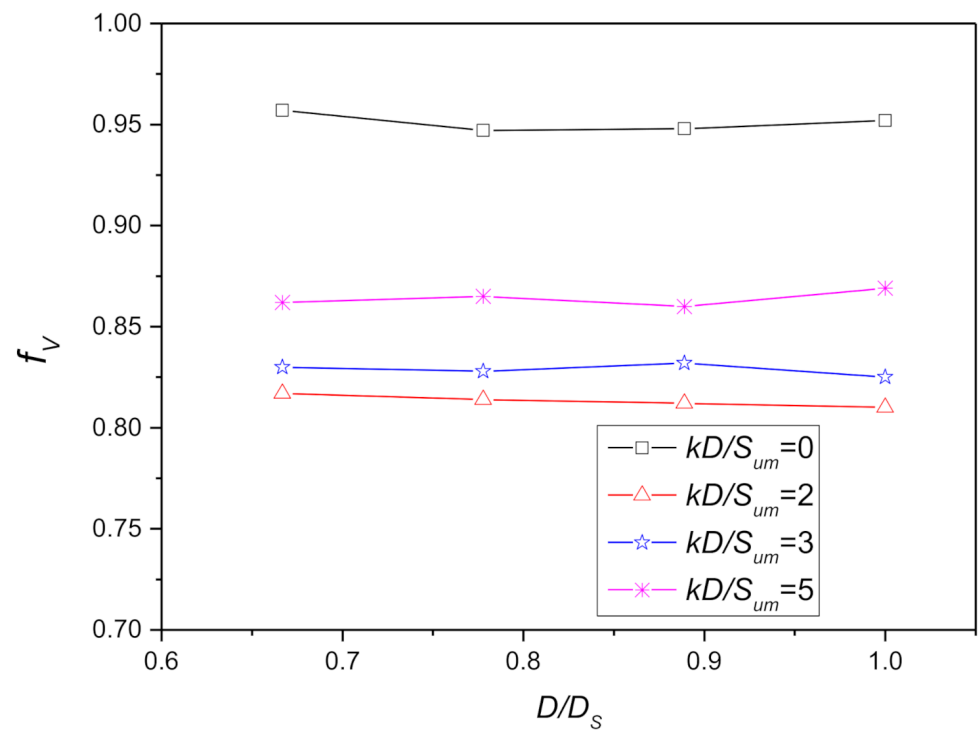
Figure 20. Influence of $\frac{kD}{S_{um}}$ and $\frac{D}{D_s}$ on f_V when $\frac{w}{D} = 1$.
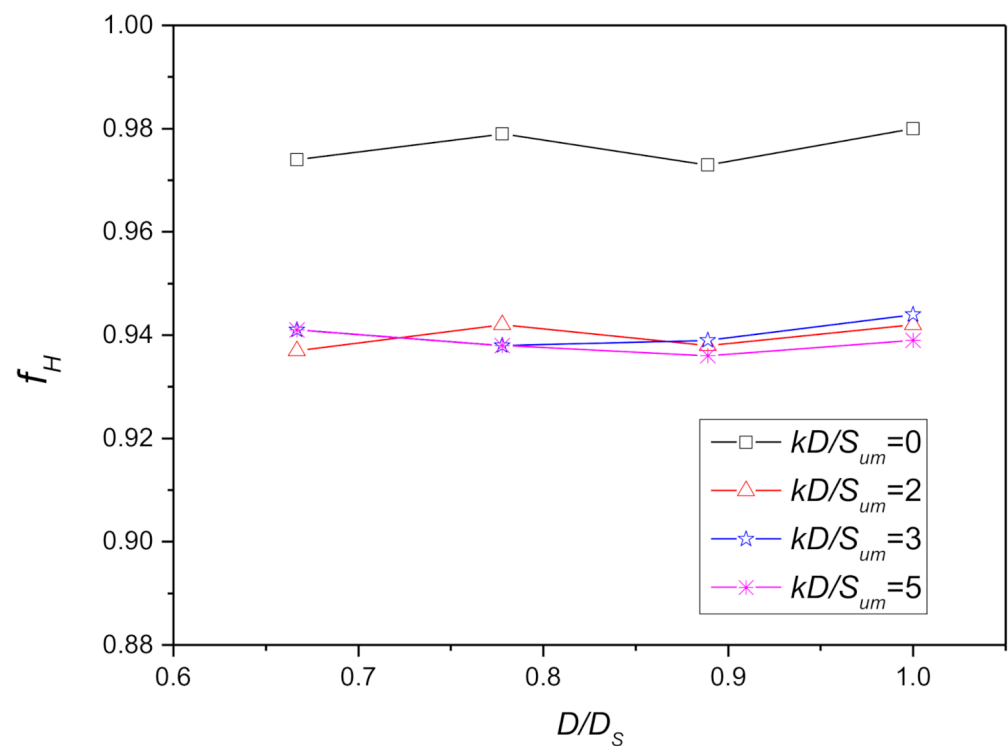
Figure 21. Influence of $\frac{kD}{S_{um}}$ and $\frac{D}{D_s}$ f_H when $\frac{w}{D} = 1$.
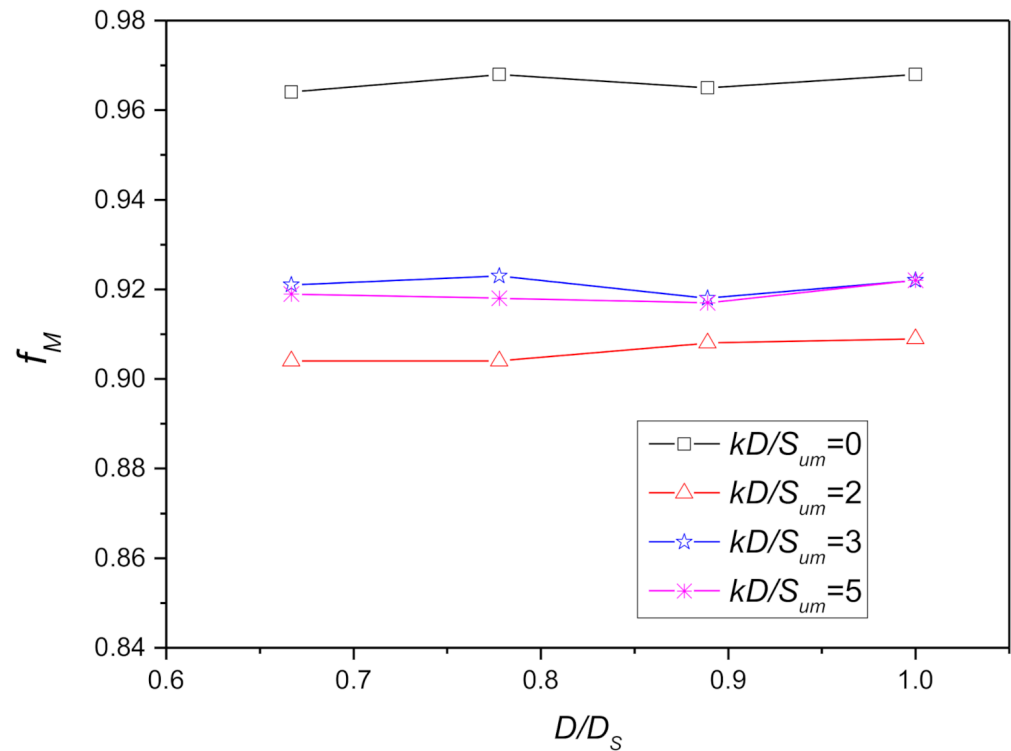
Figure 22. Influence of $\frac{kD}{S_{um}}$ and $\frac{D}{D_s}$ on f_M when $\frac{w}{D} = 1$

The entire database provides the basis for the mathematical fitting exercise, which yields the following equations to reflect the joint influences of $\frac{KD}{S_{um}}$ and $\frac{w}{D}$:

$$f_V = 0.96 - \frac{\left| \sin 0.4 \left(\frac{kD}{S_{um}} \right)^{1.5} \right|}{0.5 * \left(\frac{kD}{S_{um}} + 1 \right)^2} - \frac{0.2}{\frac{wS_{um}}{kD^2} + 2.5} \tag{7}$$

$$f_H = 0.98 - \frac{0.1 \left(1 + \sqrt{\frac{w}{D}} \right) \left(\frac{kD}{S_{um}} \right)^{0.2}}{2 + \left(\frac{kD}{S_{um}} \right)^{0.2}} + \frac{0.1 \sqrt{\frac{kD}{S_{um}}}}{3 + \frac{kD}{S_{um}}} \tag{8}$$

$$f_M = 0.98 - 0.02 \frac{w}{D} - \frac{0.3 \left(\frac{kD}{S_{um}} \right)^{0.2}}{1 + \left(\frac{kD}{S_{um}} \right)^{0.2}} + \frac{0.6 \sqrt{\frac{kD}{S_{um}}}}{5 + \frac{kD}{S_{um}}} \tag{9}$$

By and large, the fitted expression above can broadly capture the dependence of f_V, f_H, and f_M on $\frac{kD}{S_{um}}$ and $\frac{w}{D}$, as shown in Figures 23–25, although there is somewhat of a discrepancy between the fitted curves and the calculation results, in particular in Figure 23. To further assess the accuracy of these fitted equations, the 16 validation computations (Table 4) are taken advantage of. The comparison between the calculations results and estimations from these equations (Equations (7)–(9)) are detailed in Tables 11–13, where the latter are denoted by f'_V, f'_H, and f'_M to differ from the finite element calculations ones (f_V, f_H, and f_M).
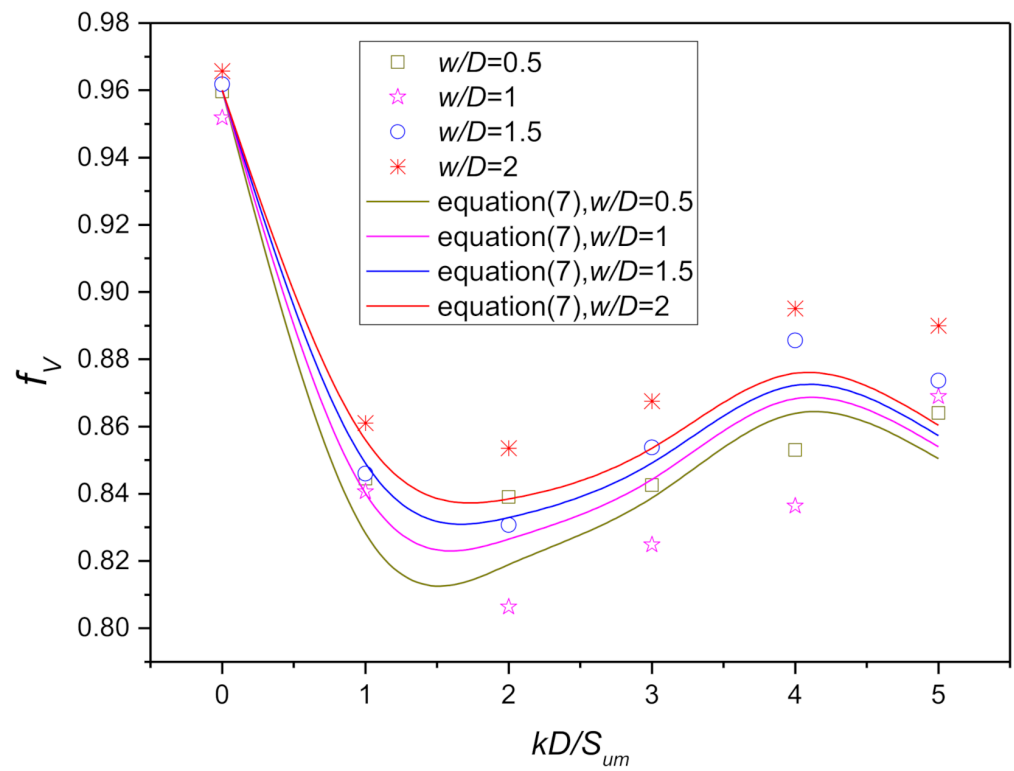
Figure 23. Reduction factors of vertical dimensionless elastic stiffness coefficients related to $\frac{kD}{S_{um}}$ and $\frac{w}{D}$.
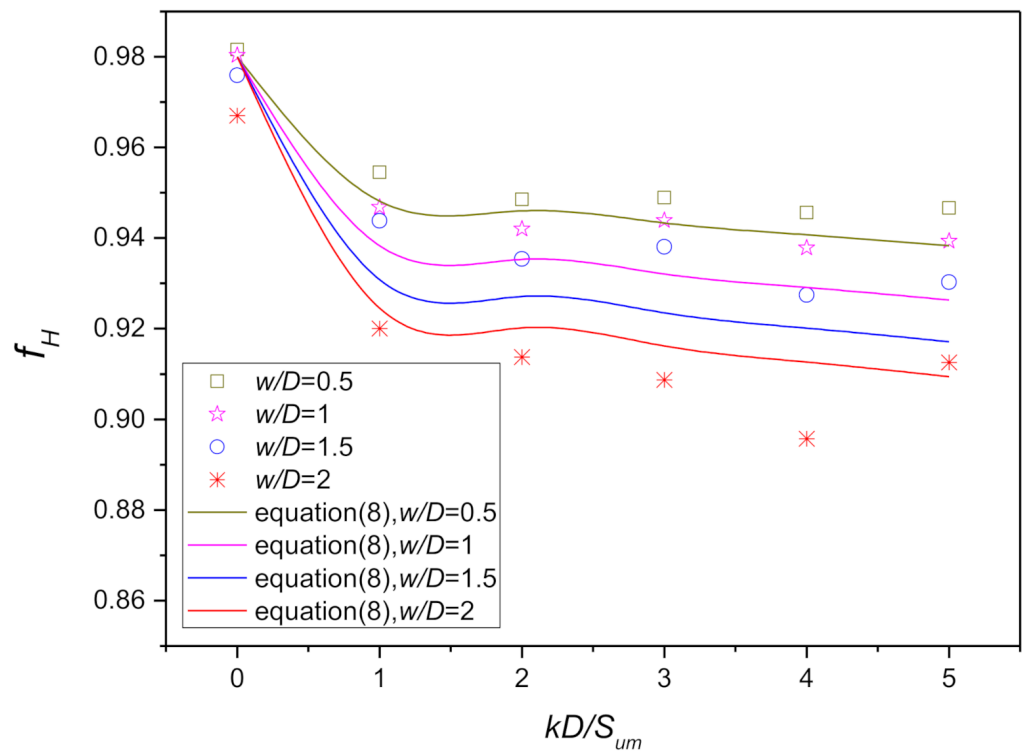
Figure 24. Reduction factors of horizontal dimensionless elastic stiffness coefficients related to $\frac{kD}{S_{um}}$ and $\frac{w}{D}$.
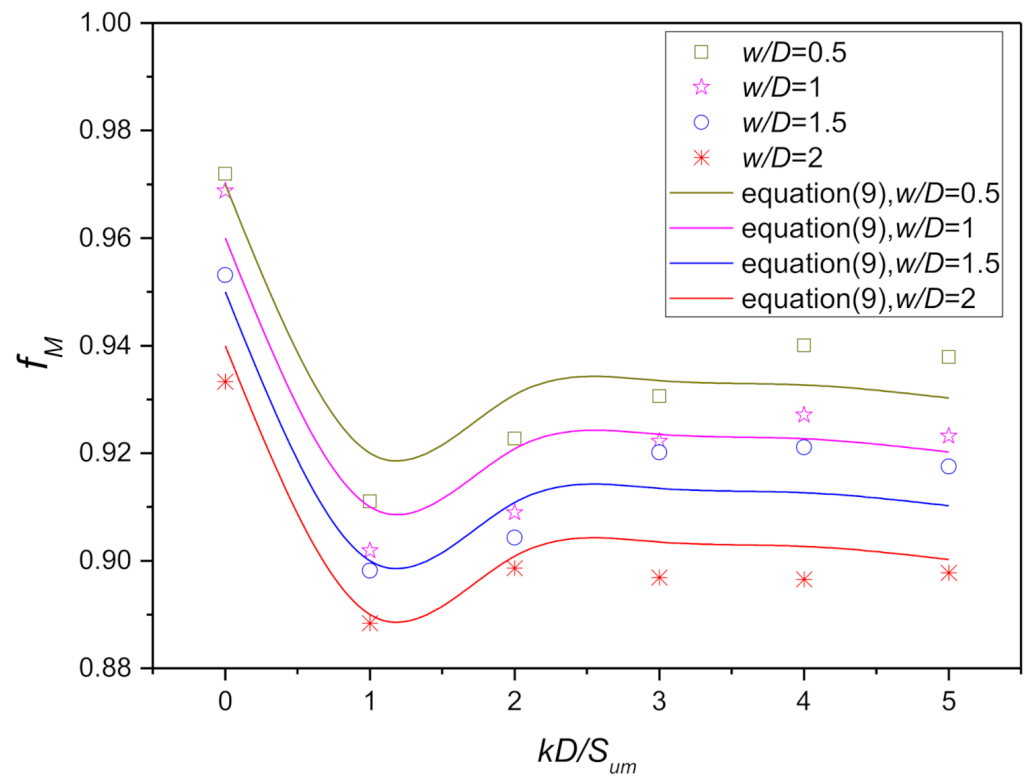
Figure 25. Reduction factors of moment dimensionless elastic stiffness coefficients related to $\frac{kD}{S_{um}}$ and $\frac{w}{D}$.

Table 11. Comparison between the reduction factors of vertical stiffness from fitted expressions and finite element analyses.

Test Number	f_V	f'_V	Difference (%)
Test 1	0.889	0.913	2.69
Test 2	0.914	0.925	1.18
Test 3	0.968	0.931	−3.74
Test 4	0.912	0.935	2.58
Test 5	0.918	0.911	−0.81
Test 6	0.973	0.939	−3.55
Test 7	0.914	0.921	0.77
Test 8	0.934	0.913	−2.21
Test 9	0.898	0.912	1.62
Test 10	0.893	0.916	2.52
Test 11	0.986	0.949	−3.78
Test 12	0.879	0.934	6.36
Test 13	0.860	0.911	6.00
Test 14	0.888	0.914	2.89
Test 15	0.896	0.951	6.11
Test 16	0.907	0.958	5.64

3.3. A workable Example: A Illustration of Significance of Installation Effects

To illustrate the practical implications of the preceding research outcomes, a workable example is presented in this section. In this example, a spudcan with a 14m diameter is embedded at a depth of 36m below a normally consolidated soil clayey seabed, where the soil shear strength profile takes the form $S_u = 7.5 + 1.11z$ kPa. For this situation, it can thus be readily derived that the embedment ratio $\frac{w}{D} = 2.571$, the non-homogeneity factor $\frac{KD}{S_{um}} = 2.072$, and the size coefficient $\frac{D}{D_s} = 0.778$. With these, the elastic stiffness coefficient without the consideration of the installation effects can be figured out from the

preceding Equations (3)–(5), whereas these after considering the installation effects can be estimated from the above Equations (6)–(8). As shown in Table 14, the consideration of installation effects can lead to the reduction in elastic stiffness coefficients by approximately 8.7% to 11.0%. In other words, the ignorance of installation effects would overestimate the spudcan stiffness by the aforementioned amounts. However, this may differ from one case to another. With the fitted expression (i.e., Equations (6)–(8)) provided in the present work, one can figure out for the situation of one's interest.

Table 12. Comparison between the reduction factors of horizontal stiffness from fitted expressions and finite element analyses.

Test Number	f_H	f'_H	Difference (%)
Test 1	0.935	0.942	0.71
Test 2	0.944	0.935	−1.05
Test 3	0.973	0.930	−4.42
Test 4	0.938	0.927	−1.22
Test 5	0.937	0.912	−2.69
Test 6	0.883	0.917	3.79
Test 7	0.958	0.937	−2.19
Test 8	0.914	0.948	3.69
Test 9	0.913	0.930	1.82
Test 10	0.936	0.945	0.90
Test 11	0.949	0.905	−4.69
Test 12	0.906	0.924	1.90
Test 13	0.937	0.920	−1.78
Test 14	0.947	0.913	−3.58
Test 15	0.931	0.940	1.02
Test 16	0.907	0.920	1.34

Table 13. Comparison between the reduction factors of moment stiffness from fitted expressions and finite element analyses.

Test Number	f_M	f'_M	Difference (%)
Test 1	0.877	0.920	4.97
Test 2	0.886	0.900	1.55
Test 3	0.910	0.887	−2.58
Test 4	0.846	0.878	3.78
Test 5	0.878	0.875	−0.30
Test 6	0.860	0.905	5.24
Test 7	0.871	0.905	4.00
Test 8	0.904	0.925	2.29
Test 9	0.895	0.905	1.13
Test 10	0.873	0.920	5.33
Test 11	0.880	0.894	1.66
Test 12	0.882	0.913	3.61
Test 13	0.866	0.890	2.76
Test 14	0.882	0.890	0.92
Test 15	0.910	0.932	2.39
Test 16	0.897	0.910	1.46

Table 14. Effect of spudcan installation on dimensionless initial stiffness coefficients.

	$K'_V/f'_H K'_V$	$K'_V/f'_H K'_V$	$K'_V/f'_H K'_V$
Stiffness coefficients with consideration of installation effect (Equations (3)–(5))	15.86	12.72	11.45
Stiffness coefficients with consideration of installation effect (Equations (6)–(8))	14.49	11.62	10.19
Difference (%)	−8.65	−8.7	−11.45

4. Conclusions

This study utilizes both SSFE and LDFE calculations to systematically evaluate the elastic stiffness coefficients of a spudcan. In particular, through the use of DSEL technique, successful attempts are made to simulate the spudcan penetration and the following combined VHM loading with the objective to re-evaluate dimensionless stiffness coefficients for the spudcan after the proper consideration of spudcan installation effects. The effects of strength non-homogeneity, embedment depths, and the size of spudcan are considered comprehensively. Expressions for the dimensionless elastic stiffness coefficient of spudcan are provided. It is clearly indicated that the installation of the spudcan exerts considerable influence on the elastic responses of the spudcan, which is reflected by the decrease in elastic stiffness coefficients in various directions. Reduction factors are then introduced, which can take the spudcan installation into account within the existing framework. The product of the reduction factor and the elastic stiffness coefficient thus give the elastic stiffness of spudcan foundations with consideration of spudcan installation effects. In practical applications, these coefficients can be directly input as the boundary conditions in the structural analysis to carry out the design of the spudcan. The findings from this paper may be beneficial in that they can provide practicing engineers a more rational estimation of the stiffness of a spudcan embedded in soft clay, and thus a more realistic account of soil–spudcan interaction in the structural analysis.

Author Contributions: Conceptualization, methodology, writing, verification, and software: W.-L.L.; writing, investigation, verification, and software: J.-T.Y.; verification and software: Z.W. and F.L. All authors have read and agreed to the published version of the manuscript.

Institutional Review Board Statement: Not applicable.

Informed Consent Statement: Not applicable.

Data Availability Statement: Data is available from the authors upon reasonable request.

Conflicts of Interest: The authors declare no conflict of interest to the work submitted.

References

1. Cassidy, M.J.; Vlahos, G.; Hodder, M. Assessing appropriate stiffness levels for spudcan foundations on dense sand. *Mar. Struct.* 2010, *23*, 187–208. [CrossRef]
2. de Santa, M.; Lima, P.E. Behaviour of Footings for Offshore Structures under Combined Loads. Ph.D. Thesis, University of Oxford, Oxford, UK, 1988.
3. Cassidy, M.J.; Eatock, T.; Houlsby, G.T. Analysis of jack-up units using a constrained NewWave methodology. *Appl. Ocean Res.* 2001, *23*, 221–234.
4. Cassidy, M.J.; Taylor, P.H.; Taylor, R.E.; Houlsby, G.T. Evaluation of long-term extreme response statistics of jack-up platforms. *Ocean Eng.* 2002, *29*, 1603–1631.
5. Poulos, H.G.; Davis, E.H. *Elastic Solutions for Soil and Rock Mechanics*; John Wiley & Sons: New York, NY, USA, 1974; Volume 582.
6. Bell, R.W. The Analysis of Offshore Foundations Subjected to Combined Loading. Master's Thesis, University of Oxford, Oxford, UK, 1991.

7.   Ngo-Tran, C. The Analysis of Offshore Foundations Subjected to Combined Loading. Ph.D. Thesis, University of Oxford, Oxford, UK, 1996.

8.   Selvadurai, A.P.S. The settlement of a rigid circular foundation resting on a half-space exhibiting a near surface elastic non-homogeneity. *Int. J. Numer. Anal. Methods Geomech.* 1996, *20*, 351–364.

9.   Doherty, J.P.; Deeks, A.J. Elastic response of circular footings embedded in a non-homogeneous half-space. *Géotechnique* 2003, *53*, 703–714.

10. Zhang, Y.; Cassidy, M.J.; Bienen, B. Elastic stiffness coefficients for an embedded spudcan in clay. *Comput. Geotech.* 2012, *42*, 89–97.

11. Zhang, Y.; Wang, D.; Cassidy, M.J.; Bienen, B. Effect of installation on the bearing capacity of a spudcan under combined loading in soft clay. *J. Geotech. Geoenviron. Eng.* 2014, *140*, 04014029.

12. ISO. *ISO 19905-1. Petroleum and Natural Gas Industries—Site-Specific Assessment of Mobile Offshore Units—Part 1: Jack-Ups*; ISO: Geneva, Switzerland, 2016.

13. Hu, Y.; Randolph, M.F. H-adaptive FE analysis of elasto-plastic non-homogeneous soil with large deformation. *Comput. Geotech.* 1998, *23*, 61–83.

14. Peng, Y.; Ding, X.; Zhang, Y.; Wang, C.; Wang, C. Evaluation of the particle breakage of calcareous sand based on the detailed probability of grain survival: An application of repeated low-energy impacts. *Soil Dyn. Earthq. Eng.* 2021, *141*.

15. Peng, Y.; Liu, H.; Li, C.; Ding, X.; Deng, X.; Wang, C. The detailed particle breakage around the pile in coral sand. *Acta Geotech.* 2021. [CrossRef]

16. Zhang, Y.; Bienen, B.; Cassidy, M.J.; Gourvenec, S. The undrained bearing capacity of a spudcan foundation under combined loading in soft clay. *Mar. Struct.* 2011, *24*, 459–477.

17. Yi, J.T.; Zhao, B.; Li, Y.P.; Yang, Y.; Lee, F.H.; Goh, S.H.; Zhang, X.Y.; Wu, J.F. Post-installation pore-pressure changes around spudcan and long-term spudcan behaviour in soft clay. *Comput. Geotech.* 2014, *56*, 133–147.

18. Hossain, M.S.; Randolph, M.F. New mechanism-based design approach for spudcan foundations on single layer clay. *J. Geotech. Geoenviron. Eng.* 2009, *135*, 1264–1274.

19. Liu, F.; Yi, J.; Cheng, P.; Yao, K. Numerical simulation of set-up around shaft of XCC pile in clay. *Geomech. Eng.* 2020, *21*, 489–501.